Analysis of coastal eddies in the Gulf of Naples

Leonardo Bagaglini

Master in Meteorologia e Oceanografia Fisica 2017/2018

Università degli Studi di Napoli Parthenope e del Salento

leonardo.bagaglini@gmail.com

Abstract

We test three different eddy detection algorithms on HF radar observations relative to the Gulf of Naples. The first two algorithms are adapted versions of those developed by Nencioli et al. [3], and Le Vu et al. [1]. The third method, developed by us, tries to deal with the problems arising from the highly non-geostrophy of the flow; relatively to our dataset it is able to compute about 30% more eddies than the previous ones. Also, we study the eddy characteristic shape, size and spatial distribution.

Introduction

Submesoscale eddies are the most frequent turbulent phenomena occurring throughout the ocean. However, due to their small length scale (1-10 km) and time scale (1-2 h), they are extremely volatile. They primary act as energy conveyors from the mesoscale to the microscale, according to the Kolmogorov's theory, but they also perform a crucial ecological role by influencing the local circulation. Typically their relative Rossby number Ro is equal or greater than unity, making difficult a theoretical treatment of such phenomena; for eddies inhabiting the Gulf of Naples $\mathrm{Ro} \sim 0.6$.

Dataset

We used HF radar observations (November 24 - December 8, 2008) of surface currents in the Gulf of Naples, hereafter GoN, produced by a CODAR (Coastal Ocean Dynamics Application Radar) SeaSonde system (see Figure 1). Since the observed GoN eddies have radii in a range between 0.5 and 5 km, we refined the grid increasing the spatial resolution up to 0.5 km by using cubic interpolations.

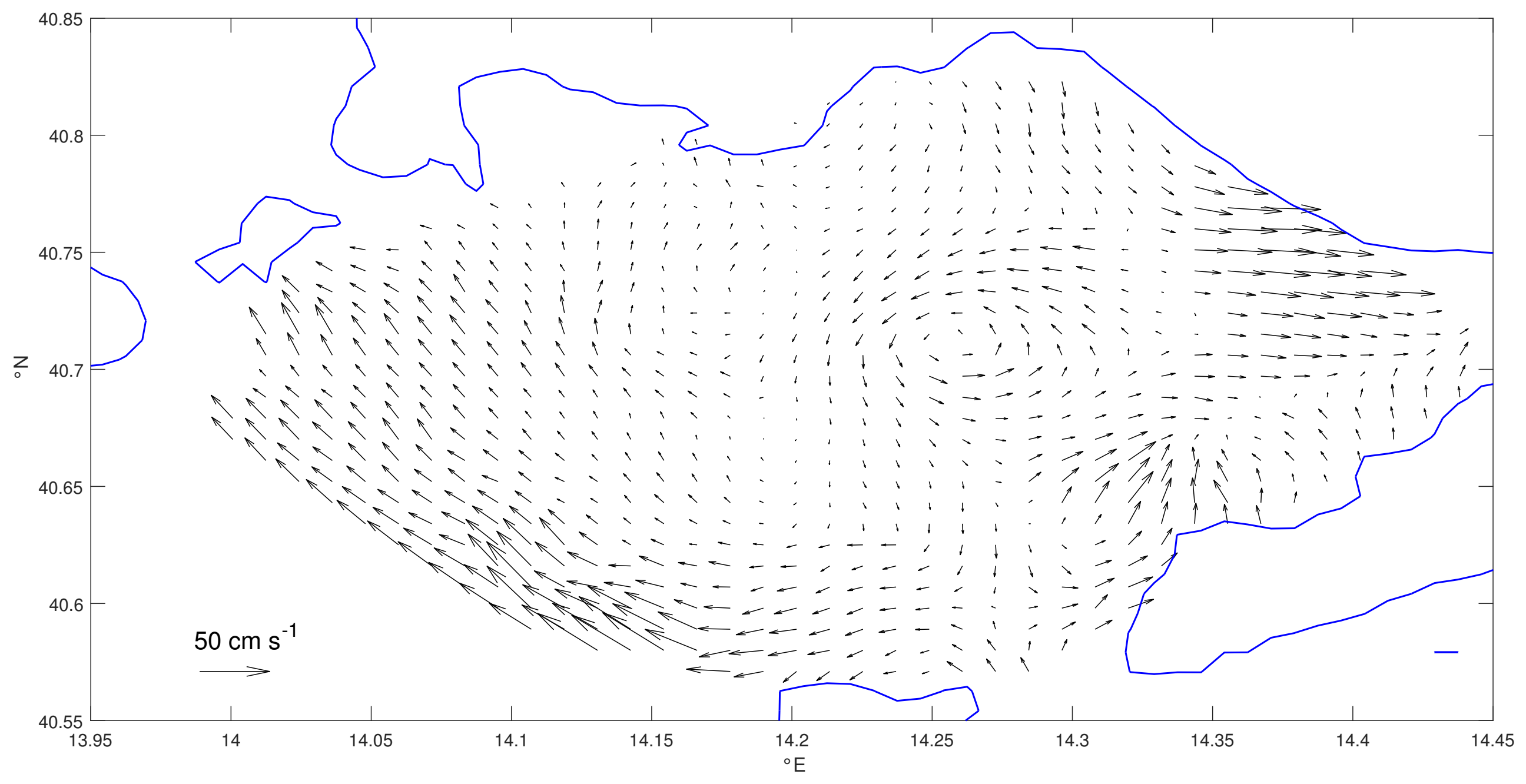

Figure 1: GoN surface currents produced by the HF radar observations. Black arrows and blue lines denote the velocity field and the coastline respectively.

Existing algorithms

We tested two algorithms adapted from [3] and [1] to our dataset. After having tuned the first we tried to to the same with the second: unfortunately we did not manage to decide the optimal parameters choice. This difficulty was likely caused by eddies having highly deformed shapes.

The first algorithm identifies eddy cores as angular momentum local extrema, without taking account of local divergences. To avoid to select eddies having diverging orbits, therefore, we chose extrema within a given threshold of outgoing momentum flux, obtaining a number of detected eddies equal to 196.

The new algorithm

Our algorithm identifies angular momentum local extrema as potential *Eddy Extreme Points*, hereafter EEPs. It then computes the streamlines emanated by increasing circles centred at the EEP. A streamline is *admissible* if 1) it stays away from the boundary and 2) it completes at least one revolution in the plane. If no admissible streamlines are detected the circle radius is increased by one pixel length. Once a circle having admissible streamlines is found the algorithm compute the streamlines end points and mean points. We expect that in presence of a sink-like core the end points will accumulate near it, otherwise, namely in presence of elliptic orbits, the mean points will do. So the algorithm selects the distribution with less variance and compute its mean point, which is labelled as the *Eddy Symmetry Centre*, shortly ESC. However, to ensure us we are not selecting an eddy relative to some other extremum we check that the expected ESC belongs to the disk bounded by the chosen circle. This new algorithm detected 255 eddies, about 30% more eddies than the first one.

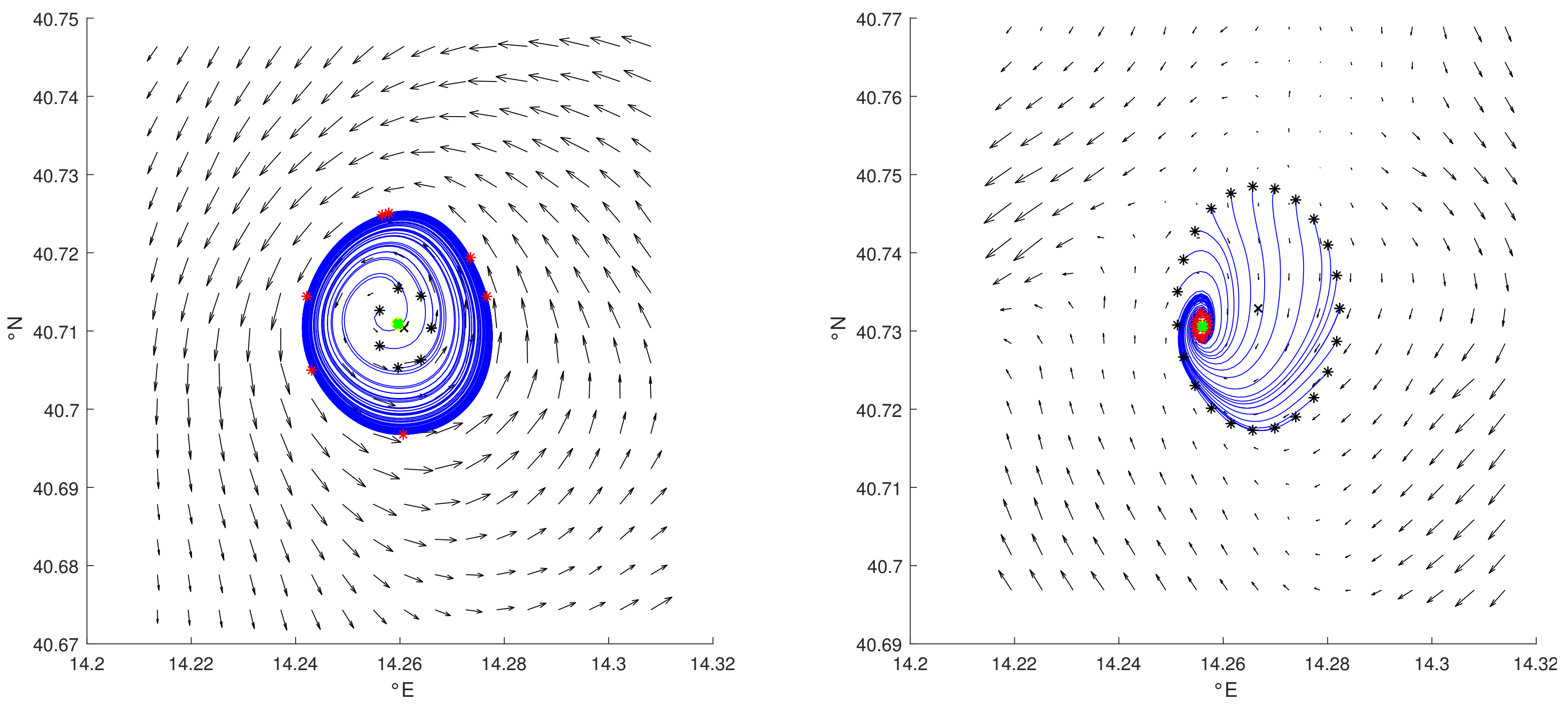

Figure 2: Maps showing two detected eddies, one having stable orbits (on the left) and the other having hyperbolic orbits (on the right). The algorithm checks whether there exist circles (black stars) centered at the EEPs (black crosses) emitting admissibile streamlines (blue lines). Streamlines end points and mean points in red and yallow respectively, ESCs in green.

Boundaries

Our algorithm looks for elliptical boundaries so, once the admissible streamlines are identified, it computes the eccentricity e of their variance ellipse. It then analyses the streamlines emanated by the ellipses E_d with eccentricity e and semi-major axis d, for $d = l, 2l, \dots, d^*$, being d^* the maximum value making the circulation along E_d an increasing function of d. For eddies with sink-like cores the algorithm selects the largest ellipse having no streamline leaving the domain as boundary, as shown in Figure 3. For eddies with elliptic orbits, instead, it chooses the ellipse with the largest d for which the ellipse is weakly deformed by the flow (seeing at the Hausdorff distance) and the circulation does not decrease, as shown in Figure 4.

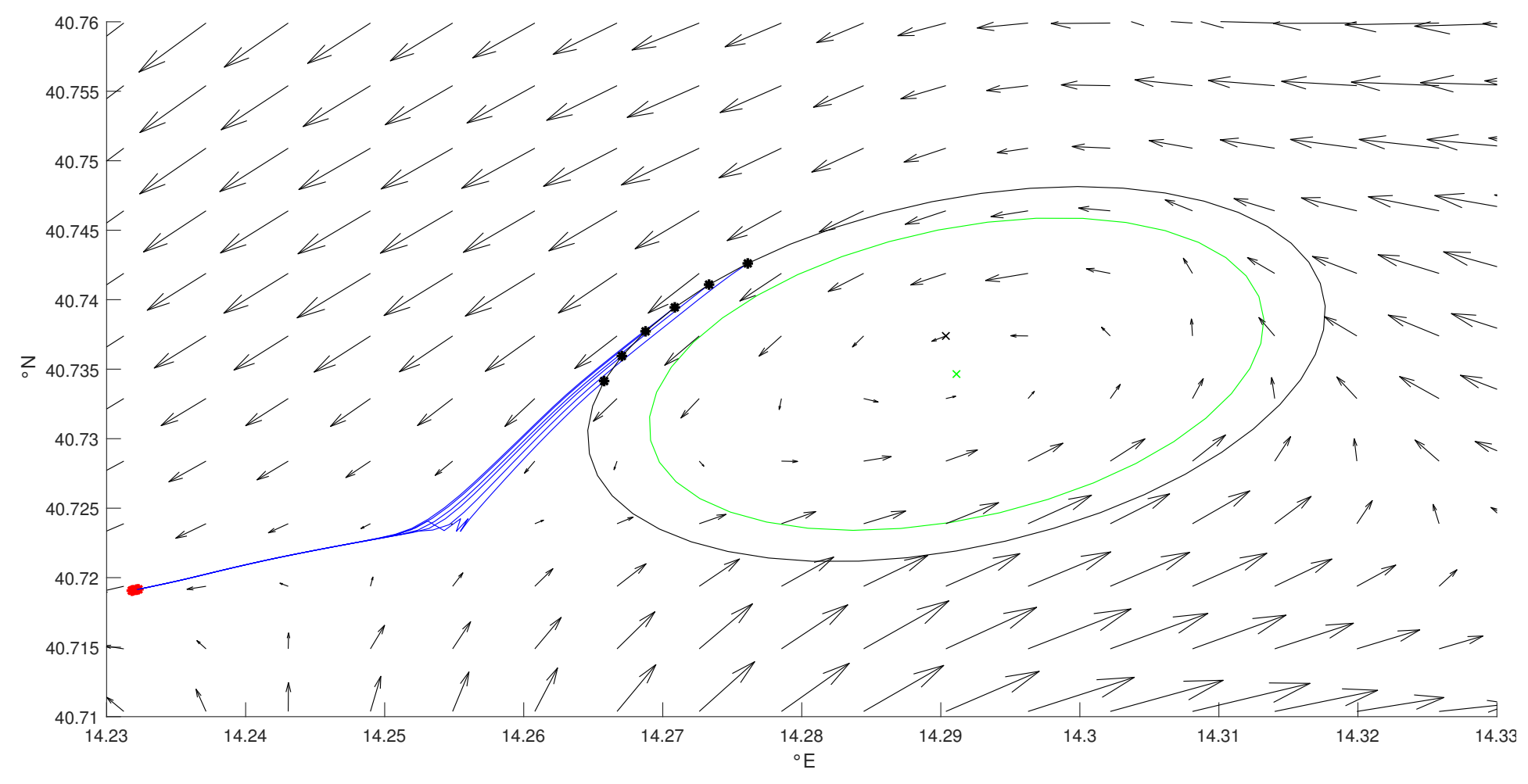

Figure 3: Map showing the boundary computation for an eddy having hyperbolic orbits. We choose the sharpest and largest ellipse (green line) centered at the ESC (green cross) emitting no diverging streamlines. The greater ellipse (black line) emanates streamlines (blue lines) leaving the region (starting points in black and contact points in red). The black cross denotes the EEP.

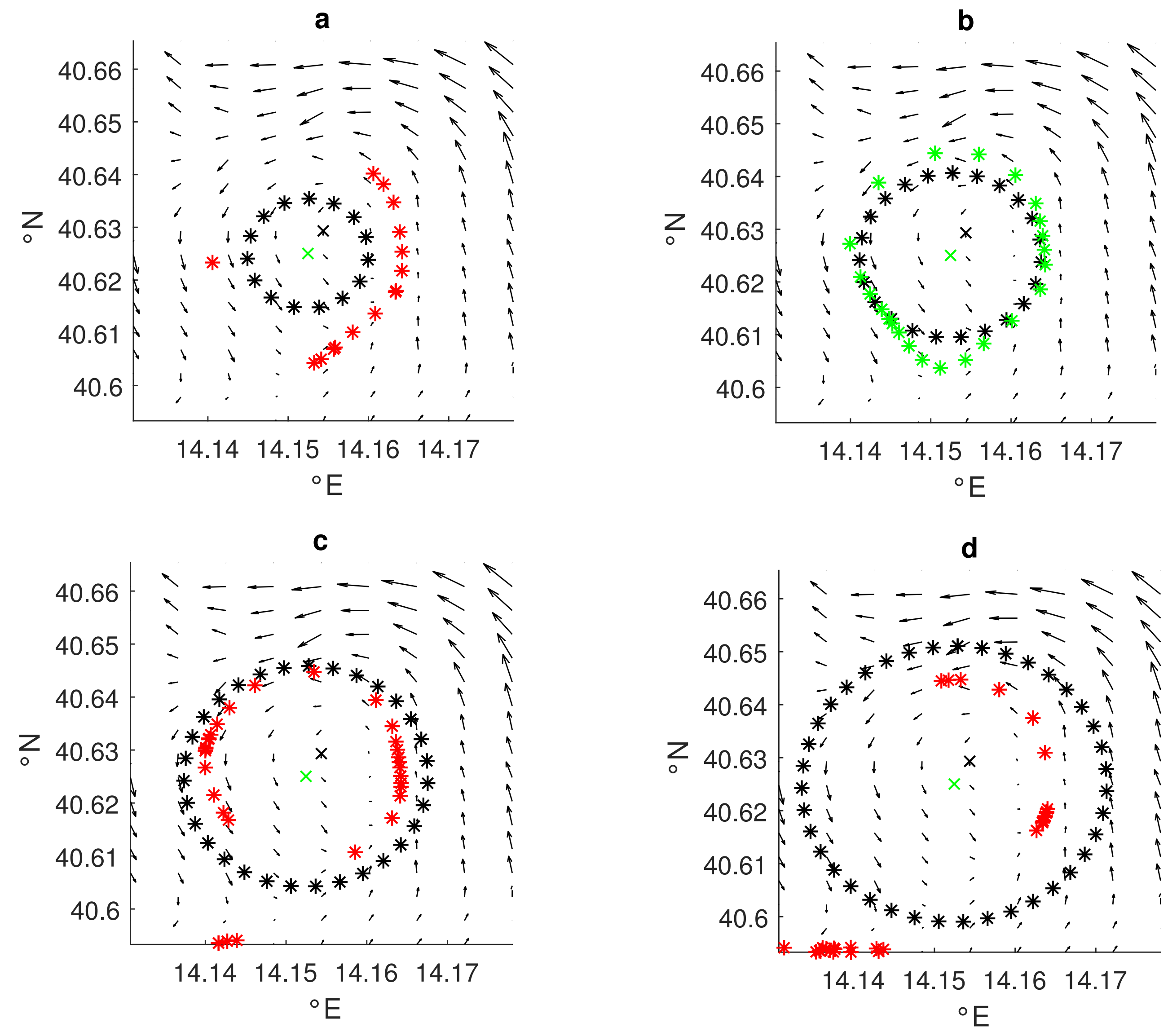

Figure 4: Map showing the boundary computation for an eddy having elliptic orbits. Once the Eddy Extreme Point EEP (black cross) and the Eddy Symmetry Center ESC (green cross) are detected the algorithm draws the ellipses centred at the ESC with increasing semi-major axis (black stars). It then evaluates the end points (red stars in figures a,b and d, and green stars in c) of the streamlines emanated by these ellipses. The algorithm selects the semi-major axis for which the relative end points (green stars in c) form the closest deformation of the associated ellipse.

Equivalent radius and spatial distribution

For each detected eddy we computed the *equivalent eddy radius* ρ, which is the radius of the circle bounding an area equivalent to that delimited by the boundary. We found a mean equivalent radius $\overline{\rho} = 0.84$ km and a mean eccentricity $\overline{e} = 0.71$. We also computed the spatial distribution of the detected eddies in Figure 5. It turns out that the largest density is achieved in correspondence of a plateau at 160 m of depth.

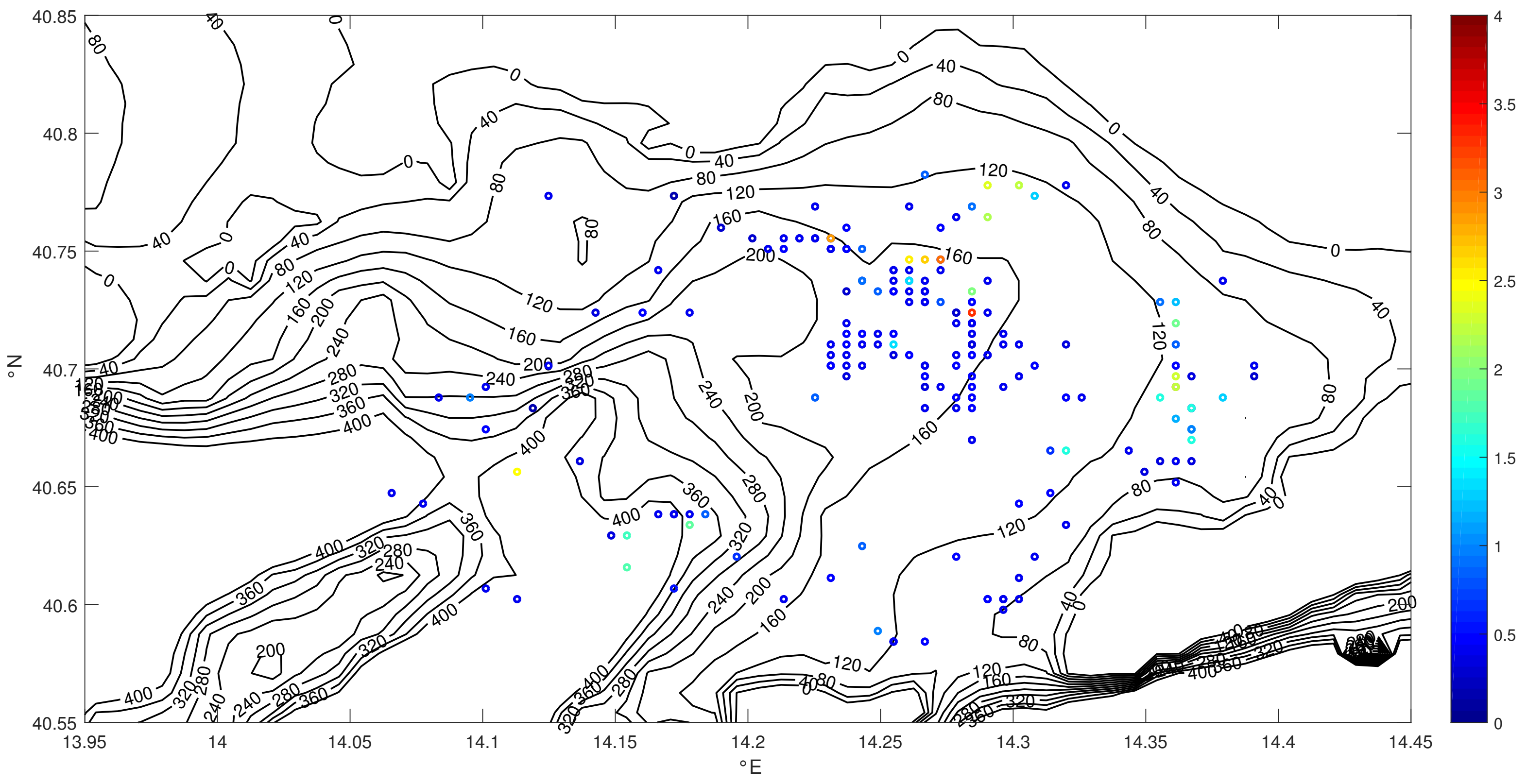

Figure 5: Spatial distribution of detected eddies (coloured circles); different colors denote different sizes. Bathymetry lines [m] (black lines) from GEBCO.

Conclusions

The chosen existing eddy detection algorithms are designed for being applied to geostrophic or quasi-geostropich flows. Consequently they do not efficiently adapt to our dataset. The algorithm developed by us detects, and distinguishes, different types of eddies. Also, it estimates the eddy center position more precisely. Further the method for estimating eddy boundaries seems to be quite accurate. However, the computed mean equivalent radius turns to be small, about 1-2 times the pixel length. Finally we observed the largest density of detected eddies in proximity of a plateau, at 160 m of depth.

References

[1] Le Vu et al. Angular Momentum Eddy Detection and tracking Algorithm (AMEDA) and its application to coastal eddy formation. J. of Atmospheric and Oceanic Technology. DOI: 10.1175/JTECH-D-17-0010.1. Volume 35, 739-762, 2017.

[2] Mkhinini et al. Long-lived mesoscale eddies in the eastern Mediterranean Sea: Analysis of 20 years of AVISO geostrophic velocities. J. Geophys. Res. Oceans, 119, 8603–8626, https://doi.org/10.1002/2014JC010176, 2014.

[3] Nencioli et al. A Vector Geometry–Based Eddy Detection Algorithm and Its Application to a High-Resolution Numerical Model Product and High-Frequency Radar Surface Velocities in the Southern California Bight. J. of Atmospheric and Oceanic Technology. DOI: 10.1175/2009JTECHO725.1. Volume 27, 564-579, 2008.